Magnetic force microscopy study of interlayer kinks in individual vortices in the underdoped cuprate superconductor $YBa_2Cu_3O_{6+x}$

Lan Luan,[1] Ophir M. Auslaender,[1] Douglas A. Bonn,[2] Ruixing Liang,[2] Walter N. Hardy,[2] and Kathryn A. Moler[1,*]
[1]*Geballe Laboratory for Advanced Materials, Stanford University, Stanford, California 94305, USA*
[2]*Department of Physics and Astronomy, University of British Columbia, Vancouver, British Columbia, Canada V6T 1Z1*
(Received 6 May 2009; published 26 June 2009)

We use magnetic force microscopy to both image and manipulate individual vortex lines threading single crystalline $YBa_2Cu_3O_{6.4}$, a layered superconductor. We find that when we pull the top of a pinned vortex, it may not tilt smoothly. Occasionally, we observe a vortex to break into discrete segments that can be described as short stacks of pancake vortices, similar to the "kinked" structure proposed by Benkraouda and Clem. Quantitative analysis gives an estimate of the pinning force and the coupling between the stacks. Our measurements highlight the discrete nature of stacks of pancake vortices in layered superconductors.

DOI: 10.1103/PhysRevB.79.214530 PACS number(s): 74.72.−h, 68.37.Rt, 74.25.Qt

I. INTRODUCTION

Magnetic field penetrates superconductors in the form of vortices, each carrying one magnetic flux quantum, $\Phi_0 \equiv h/2e$ (h is the Planck constant and $-e$ is the electron charge). In highly anisotropic cuprates, where the c-axis penetration depth (λ_c) is much larger than the in-plane penetration depth (λ_{ab}), a vortex can be treated as a stack of two-dimensional, magnetically coupled, "pancake" vortices,[1,2] with weak interlayer Josephson coupling.[3,4] Rich physics arises from the competition between thermal energy, vortex-vortex interactions, pinning, and interlayer coupling. While there are numerous studies on vortex matter thermodynamics,[5] work on individual vortices is scarce. Here we use a magnetic force microscope (MFM) to directly probe the pinning energy and interlayer coupling of an individual vortex, both of which determine its shape and the nature of its motion.

The pancake model is a well-accepted description for vortices in layered superconductors.[5] Many macroscopic measurements have confirmed this picture, e.g., by observing the loss of vortex line tension at high magnetic fields and elevated temperatures.[6,7] On the single vortex level, Benkraouda and Clem proposed that the sheared pancake vortices can break into separate straight stacks of pancakes to create a kinked structure instead of tilting[8] [Fig. 1(a)]. This "kinking" model has been used to explain magnetic features with sub-Φ_0 flux observed in images of individual vortices[9–11] and to study the interaction between pancake vortices and interlayer Josephson vortices.[11,12]

MFM has an important advantage over other magnetic imaging techniques in that it allows us to also manipulate individual vortices[13] with nanoscale control and a known force.[14,15] Our previous work[15] demonstrated that in an overdoped $YBa_2Cu_3O_{6.991}$ single crystal, a vortex follows the MFM tip as the tip moves back and forth over it and exhibits a marked enhancement of the motion perpendicular to this wiggling direction. In $YBa_2Cu_3O_{6.991}$ vortices behave like elastic strings rather than stacks of pancakes due to the moderate anisotropy ($\gamma \equiv \lambda_c^{T=0K}/\lambda_{ab}^{T=0K} \approx 5-7$).[5] Here we need larger anisotropy because our goal is to provide a direct test for the "kinking" model and, by implication, for the discrete nature of pancake stacks. We therefore use a very underdoped $YBa_2Cu_3O_{6+x}$ (YBCO) single crystal, because it is known that reducing the doping increases the anisotropy[16] and decreases the interlayer coupling.

In the experiment we create and annihilate interlayer "kinks" with the MFM and measure the coupling between pancake stacks. We first map the magnetic interaction of the MFM tip with the magnetic field from the sample. Occasionally we observe pairs of well-separated features carrying sub-Φ_0 flux, similar to those interpreted in the past as kinked pancake stacks stabilized by local pinning.[9] We then use the MFM tip to combine these pairs of features to create regular Φ_0 vortices. Our success verifies the kinking model. As an even more stringent test, we split regular Φ_0 vortices by pulling them apart to create kinks. We determine the required force, which gives an estimate for the attractive interaction between pancake stacks. The result agrees well with the pancake model with dominant magnetic coupling augmented by the line tension of the Josephson string connecting the stacks.

II. SAMPLE AND TECHNIQUE

The 100 μm thick platelet shaped crystal $YBa_2Cu_3O_{6+x}$ (0.7 mm × 0.7 mm face ∥ crystal ab-plane) was grown by the self-flux method in $BaZrO_3$ crucibles,[17] mechanically detwinned and annealed. $T_c = 21$ K (transition width $\Delta T_c \approx 2$ K), implying $x \approx 0.4$ and thus $\lambda_{ab}^{T=0K} \approx 0.36$ μm and anisotropy $\gamma \approx 75$,[18–20] comparable to $Bi_2Sr_2CaCu_2O_{8+x}$ ($\gamma \approx 60-250$).[5]

Our measurements were performed in a variable temperature MFM in frequency modulation mode.[21] In the experimental setup, a commercial magnetic tip at the end of a flexible cantilever[22] faces the crystal a-b plane. The tip-sample force induces a shift of the cantilever's resonant frequency f_0, which we measure. The resonant frequency changes rapidly as the tip approaches the sample, giving precise determination of the tip-sample separation. In our scans, the tip moves at a constant height z above the surface ($\hat{z} \parallel$ crystal c-axis), back and forth along $\hat{x}$. Then, after one period of motion, which lasts a few seconds, it is incremented along $+\hat{y}$ or $-\hat{y}$. The choice of $\hat{x}$ and $\hat{y}$ are illustrated in [Fig. 1(b)].

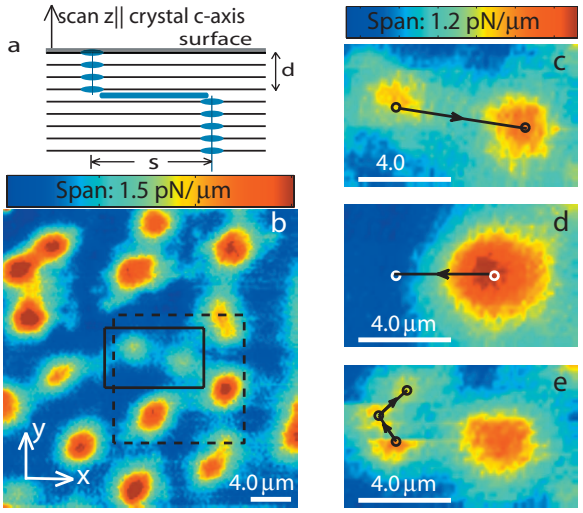

FIG. 1. (Color) MFM images showing the annihilation and creation of kinked stacks of pancake vortices, which appear as pairs of sub-Φ_0, isolated features. (a) Cartoon of a side view of a kinked pancake stack (ellipses), including the core of the vortex (vertical lines) and the interlayer Josephson vortex (thick blue line). d-depth of the kinked structure, s-lateral separation between the stacks. Also depicted are the CuO_2 layers (horizontal lines). (b) Initial configuration of vortices after field cooling from $T > T_C$ to $T = 5.4$ K. Scan height $z = 1.05$ μm. Most of the features in this scan are Φ_0 vortices. There are also what appear to be sub-Φ_0 features, referred as partial vortex stacks. The solid frame shows the scan area for Figs. 1(c)–1(e) and highlights a pair of partial stacks. The dashed frame shows the scan area for Fig. 2. Also plotted are the scanning x, y axes. [(c)–(e)] Scans at $T = 12$ K of the two stacks in the solid frame in (b). The arrows show the tip path used for manipulation, as described in the text. (c) Scan before annihilation ($z = 0.93$ μm), (d) scan after annihilation and before creation ($z = 1.24$ μm), and (e) scan after creation ($z = 1.24$ μm). In (e) the tip starts scanning from the bottom left corner and is incremented along $+\hat{y}$ after each raster period. The vortex stack on the left jumps as the tip scans over it. The dots and arrows show positions where the stack is trapped temporarily and the trajectory of its motion. Here, F_{lat} is much smaller than the force required to move a regular vortex, indicating an unstable stack configuration.

Subtracting a z-dependent offset, we obtain the contribution to the frequency shift of the tip-vortex interaction, Δf, which gives information on the tip-vortex force, $\partial F_z/\partial z = -2k\Delta f/f_0$ ($f_0 = 59.040$ kHz, the cantilever spring constant $k = 2.7 \pm 0.1$ N/m measured by Sader's method[23]).

The force exerted by the tip on the sample is generally regarded as a drawback of MFM. Here, we magnetize the tip to give attractive tip-vortex force and use its lateral components, $\vec{F}_{\text{lat}}$, to overcome the pinning force, F_{pin}, to manipulate individual vortices. We tune $F_{\text{lat}} \equiv |\vec{F}_{\text{lat}}|$ by varying z. We first image at z where F_{lat} is insufficient to perturb the vortices, which are held static by F_{pin}. For manipulation, we reduce z to increase F_{lat}. When $F_{\text{lat}}^{\max}(z) > F_{\text{pin}}(T)$, where $F_{\text{lat}}^{\max}$ indicates the maximum F_{lat} exerted during the scan, we can manipulate a vortex. Increasing temperature, which reduces $F_{\text{pin}}(T)$, gives extra control,[14,15] up to the temperature where the vortices run away.

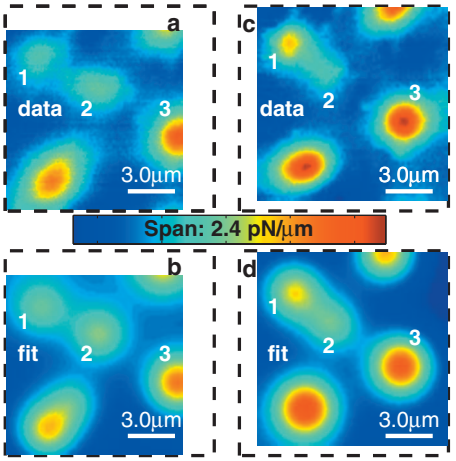

FIG. 2. (Color) Scans (a,c) and fits (b,d) of vortices before and after manipulation. The dashed frames match the dashed frame in Fig. 1(a). (a) Scan at $T = 5.3$ K, $z = 0.94$ μm, of a field cooled vortex configuration. (b) Fit to scan in (a) using the m-m model. The fitted amplitudes, $A_1 = 0.69 \pm 0.01$ pN/μm, $A_2 = 0.86 \pm 0.01$ pN/μm, $A_3 = 1.55 \pm 0.01$ pN/μm (errors denote 95% confidence intervals), give $A_1 + A_2 \approx A_3$. For pair 1-2 the fit gives $d = 0.6\lambda_{ab}$ and $s = 4.1$ μm. (c) Scan at $T = 5.3$ K, $z = 0.84$ μm, after combining and reseparating features 1 and 2. Both the signal strength and the separation between the two stacks change because of the manipulation. (d) Fit to scan in (c). Fitted amplitudes: $A_1 = 1.28 \pm 0.03$ pN/μm, $A_2 = 0.94 \pm 0.03$ pN/μm, $A_3 = 2.00 \pm 0.02$ pN/μm. As in (b), $A_1 + A_2 \approx A_3$. For this pair: $d = 0.9\lambda_{ab}$, $s = 3.2$ μm.

III. EXPERIMENT AND DISCUSSION

For low vortex density, we cool the sample in an applied magnetic field of $0.5 \cdot 10^{-4}$ T along the crystal's c-axis with the MFM tip retracted 100 μm from the sample surface (to minimize the chance of inducing vortices by the tip). Figure 1(b) shows an image acquired at $T = 5.4$ K, in which vortices appear as peaks. Most vortices give the same peak height, as expected, since they each should carry a flux of exactly Φ_0. However, some peaks have weaker amplitude and appear in pairs [e.g., Figure 1(b), solid framed region], indicating the flux associated with each member is less than Φ_0. Previous work suggests that these peaks originate from kinked stacks of pancake vortices forming one Φ_0-vortex.[9] To test this model, we annihilate kinks and recreate them [Figs. 1(c)–1(e)]. For the manipulation, we heat the sample to $T = 12$ K, reducing F_{pin}. Then, after locating two distinct partial stacks [Fig. 1(c)], we try to pull one toward the other with the tip. We repeat this until we succeed, reducing z for each new attempt (for driving to the starting position we retract the tip to reduce $F_{\text{lat}}^{\max}$, and with it the chance of accidental perturbation). We find that after we drag one vortex stack, it combines with its partner to form a Φ_0 vortex with rotational symmetry, suggesting well-aligned stacks [Fig. 1(d)]. As an additional test, we pull the vortex apart, without changing z and T, by moving the tip away from its center at $\vec{R}_i$ [Fig. 1(d)] and successfully creat two distinct stacks [Fig. 1(e)]. The newly created partial stacks are not always stable, as signified by occasional vortex jumps [Fig. 1(e)].

We confirm that the two stacks we manipulate compose one vortex by fitting the pre-annihilation scan to a model [Figs. 2(a) and 2(b)]. The model is based on the fact that, for $z \gg \lambda_{ab}$, the magnetic field from a vortex stack is approximately equal to the field from a magnetic monopole λ_{ab} below the surface of the superconductor (filling the half space $z \leq 0$):[24] $\vec{B}(\vec{R},z) \approx \frac{\beta\Phi_0}{2\pi} \frac{[\vec{R}+(z+\lambda_{ab})\hat{z}]}{[R^2+(z+\lambda_{ab})^2]^{3/2}}$, where $\vec{R}$ is the in-plane position relative to the vortex center. For a regular Φ_0 vortex, $\beta=1$. For a partial stack extending from depth d to the surface, $\beta=1-e^{-d/\lambda_{ab}}$. For a semi-infinite stack extending from d down: $\beta=e^{-d/\lambda_{ab}}$.[9] We model our tip as a long narrow cylinder magnetized along its axis $\hat{z}$. The resulting force acting on the tip due to the interaction with the vortex is $\vec{F}[\vec{R},z] \approx \tilde{m}\vec{B}[\vec{R},z]$, where $\tilde{m}$ is the dipole moment per unit length of the tip. The MFM signal from a collection of vortex stacks is then given by the "monopole-monopole" (m-m) model:

$$\partial F_z/\partial z = \sum_i A_i \frac{1-\frac{1}{2}(\vec{R}-\vec{R}_i)^2/(z+h_0)^2}{[1+(\vec{R}-R_i)^2/(z+h_0)^2]^{5/2}}, \quad (1)$$

where i enumerates the distinct vortex features in a scan, $\vec{R}$ is the in-plane position of the tip, the peak amplitude for each feature is $A_i=\beta_i\tilde{m}\Phi_0(z+h_0)^{-3}/\pi$ and $h_0=\lambda_{ab}+d_{\text{offset}}$ (d_{offset} is the offset due to the tip geometry and any non-superconducting layer on the surface of the superconductor[15]). The fit in Fig. 2(b) using Eq. (1) gives $A_1+A_2 \approx A_3$ implying $\beta_1+\beta_2=1$ and confirming that two adjacent partial vortex stacks add up to one regular vortex. We want to point out that although the monopole model for the tip is a simplification, the details of the model are not important. As long as the model describes the data and extract the amplitude of each feature correctly, it leads to the same conclusion that the two partial stacks add up to be one regular vortex.

Other experimental observations provide further insight about the kinked stacks. When we recombine and reseparate the same pair of stacks repeatedly, we can only manipulate one member. Presumably, this stack is the finite top stack. Furthermore, both the separation between the stacks and the signal amplitudes change in the annihilation-creation process (e.g., Fig. 2), indicating different kink structures. This result shows that pinning is important and that the tip allows the dragged pancakes to explore the pinning environment. Finally, partial pairs are rare [only one in Fig. 1(b)]. However, most other vortices have irregular shape, which we believe is due to the misalignment of the pancakes, too small to be resolved because of the relatively large λ_{ab}. This irregularity tends to diminish after dragging, in support of the picture that pinning hinders pancake stacks from aligning.

We next determine the coupling between stacks in a vortex from the force required to create a kink (Fig. 3). For that, we move the tip repeatedly along a line away from a regular vortex, reducing z for each new line scan [Fig. 3(d)]. We estimate F_{lat} from the m-m model (Fig. 4). For large z, the vortex remains unperturbed, implying $F_{\text{lat}}^{\max}(z) < F_{\text{pin}}(T)$. We estimate $F_{\text{pin}}(T)$ from the largest z at which we observe vortex motion, manifested by discontinuities in the line scan larger than the noise level (≈ 0.05 pN/μm)(We interpret features that are continuous as either topography or vortices). For example, at $T=10$ K we observe first motion at $z=0.36$ μm, giving $F_{\text{pin}}(T=10\text{ K}) \approx F_{\text{lat}}^{\max}(z=0.36\ \mu\text{m}) \approx 1.2$ pN. For lower scans (e.g., $z=0.24$ μm), the tip drags part of the vortex to a new position, creating two distinct stacks [Fig. 3(b)]. In order to pull a vortex apart, F_{lat} has to overcome both F_{pin} and the restoring force F_{el}, which binds the two partial stacks together. At a position where a partial stack stops following the tip, $F_{\text{lat}}^{\max} \approx F_{\text{pin}}+F_{\text{el}}$. Thus, the measured restoring force is $F_{\text{lat}}^{\max}(z=0.24\ \mu\text{m})-F_{\text{lat}}^{\max}(z=0.36\ \mu\text{m})$, giving $F_{\text{el}} \approx 0.1$ pN for $s=3.3$ μm, as identified by fitting Fig. 3(b) to the m-m model.

The restoring force, F_{el}, has two attractive contributions: the magnetic coupling between pancakes in different layers and the Josephson string-line tension. The former is obtained by summing over the magnetic interactions between all the pancakes in the two partial stacks. Benkraouda and Clem (BC)[8] calculated this force for two stacks of equal length, long on the scale of λ_{ab}. In our case, the length of the top stack, d, is of order λ_{ab}. For $s \gg \lambda_{ab}$ we obtain the BC result, suppressed by a factor of approximately $1-e^{-d/\lambda_{ab}}$, to give: $F_{\text{mag}}(s)=-\partial E_{\text{mag}}/\partial s \approx (\Phi_0/4\pi\lambda_{ab})^2[\lambda_{ab}/s-e^{-s/\lambda_{ab}}(1+\lambda_{ab}/s)][1-e^{-d/\lambda_{ab}}]$. The line tension of a Josephson string for $\lambda_{ab} < s < \lambda_c$ is: $F_J=-\partial E_J/\partial s \approx (\Phi_0/4\pi)^2(\lambda_{ab}\lambda_c)^{-1}$.[3] Given $\lambda_{ab}=0.40$ μm and $\lambda_c=31.6$ μm at $T=10$ K,[18,19] $s=3.3$ μm and $d=0.5\lambda_{ab}$ [from fitting Fig. 3(b)], we find $F_{\text{mag}}=0.09$ pN and $F_J \approx 0.02$ pN. Adding the two gives $F_{\text{tot}}=F_J+F_{\text{mag}}=0.11$ pN, in good agreement with our estimate from the measurement.

IV. CONCLUSIONS

We manipulated 20 vortices in different cooldowns all at temperatures around $T_c/2$. For each cycle, we warmed the sample to $T > T_C$ and then field cooled, sometimes changing the magnetic fields slightly, to get a different initial vortex configuration. We successfully created and observed the kinked structure in two vortices. In the remaining cases we could drag the top of the vortex but did not observe kinking. This is not unexpected: by MFM we can only manipulate pancakes that lie at most a few λ_{ab} beneath the surface because of the exponential suppression of F_{lat}. Imaging depth is also limited, because the resolution is set by $z+h_0$, the scale on which the magnetic field from a stack decays. The low rate of creating observable kinks in the limited volume defined by d and s (10%) and of observing field-cooled partial stacks (one pair in three thermal cycles) reasserts that the balance between local pinning and F_{el} is crucial for determining the alignment of the pancakes composing one vortex. It also suggests that although the distribution of pinning sites has spatial variation, it is not strongly inhomogeneous.

By using MFM for imaging and manipulation, we probe the force required to separate individual vortices into pancake stacks in a highly anisotropic superconductor, and find that the interaction between pancake stacks in a single vortex is dominated by magnetic coupling. Our experiment directly measures the line energy and the pinning force of a single vortex, which, in competition with thermal energy and

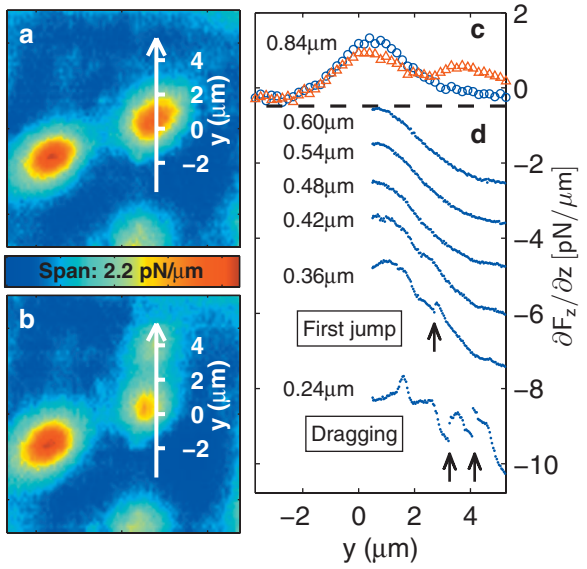

FIG. 3. (Color) Creating kinks in a straight stack. (a) Image of two regular, field cooled, vortices at $T=5.3$ K ($z=0.80$ μm). The white line marks the location of the line cut plotted in (c) and the path for the line scans in (d). (b) Image of a regular vortex [the one on the left in (a)] and the newly created kinked-stack pair, created by the sequence of line scans in (d). The white line is the same as in (a). Scan at $T=5.3$ K, $z=0.80$ μm. (c) Circles and triangles show points extracted along the white line in (a) and (b), respectively. (d) Line scans acquired with the tip moving over the white lines in (a) and (b) starting from $y=0$ ($T=12$ K). $z=0.60$, 0.54, 0.48, and 0.42 μm: the vortex is stationary at approximately $y=0$, with the signal dropping as the tip moves away. $z=0.36$ μm: the vortex jumps toward the tip for the first time [tip position when this happens is marked by an arrow, roughly when the lateral force peaks (Fig. 4)], as indicated by the abrupt signal increase due to the increased tip-vortex interaction. $z=0.24$ μm: the vortex is dragged by the tip. The arrows highlight the discontinuities of the trace due to vortex motion. We believe that other sharp features in the trace originate from bumps on the surface which would deflect the tip as we further lowered the scan height.

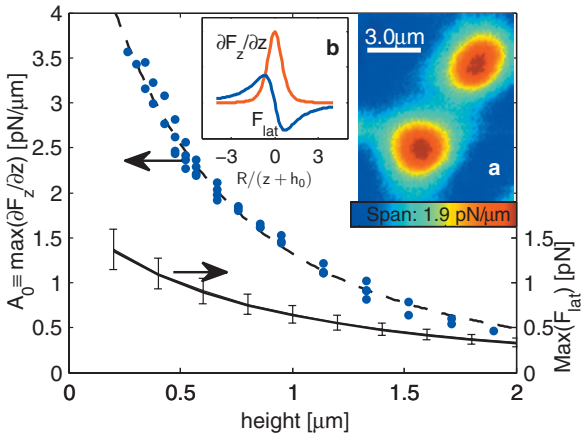

FIG. 4. (Color) Calibration of the tip to extract $F_{\mathrm{lat}}^{\mathrm{max}}(z)$, the maximum lateral force exerted on a vortex during a scan at height z. At each z we acquire a scan of two immobile vortices at $T=5.0$ K [inset (a)—an example for $z=0.85$ μm]. We fit each scan to the m-m model and plot the peak amplitude, $A_0 \equiv \max(\partial F_z/\partial z)$ (main panel, left ordinate). We then fit the result to $(\tilde{m}\Phi_0/\pi)/(z+h_0)^3$, the dependence of the peak height on z in the model (dashed line). The fit yields $\tilde{m}=22\pm3$ nA·m and $h_0=1.55\pm0.10$ μm (Ref. 25). Within the model $F_{\mathrm{lat}}^{\mathrm{max}}=(\tilde{m}\Phi_0/3\sqrt{3}\pi)/(z+h_0)^2$ (solid line, right ordinate). Error bars show the 95% confidence interval from the fit parameter uncertainty. The change of $F_{\mathrm{lat}}^{\mathrm{max}}$ due to the choice of different tip models is well within the error bars. Note that we perform the manipulation at elevated temperature (e.g., $T=10$ K for Fig. 3), which leads to an additional 10% systematic error in $F_{\mathrm{lat}}^{\mathrm{max}}$, due to the increase of λ_{ab} (Ref. 18). Inset (b) shows $\partial F_z/\partial z$ and F_{lat} in the model as a function of R in units of $(z+h_0)$. Note that $F_{\mathrm{lat}}(0)=0$ and reaches $F_{\mathrm{lat}}^{\mathrm{max}}$ at $R=(z+h_0)/\sqrt{2}$, roughly when $\partial F_z/\partial z=\max(\partial F_z/\partial z)/2$.

vortex-vortex interactions, determine the properties of vortex matter. The fact that it can be energetically cheap to form interlayer Josephson vortices in the presence of pinning implies that such vortices are less likely to entangle. Our technique of manipulating individual vortices by MFM combined with quantitative force analysis opens unique possibilities to study interacting many-body systems,[26] as well as to address open questions in vortex matter, e.g, testing vortex entanglement and measuring the cutting barrier for vortices by deliberately winding one vortex around another and determining the required force.[27,28]

ACKNOWLEDGMENTS

The authors thank H. Bluhm and B. Kalisky for helpful discussions. The work is supported by DOE under Contract No. DE-AC02-76SF00515.

*Corresponding author; kmoler@stanford.edu

[1] J. R. Clem, Phys. Rev. B **43**, 7837 (1991).
[2] S. N. Artemenko and A. N. Kruglov, Phys. Lett. A **143**, 485 (1990).
[3] J. R. Clem, J. Supercond. **17**, 613 (2004).
[4] L. N. Bulaevskii, M. Ledvij, and V. G. Kogan, Phys. Rev. B **46**, 11807 (1992).
[5] G. Blatter, M. V. Feigel'man, V. B. Geshkenbein, A. I. Larkin, and V. M. Vinokur, Rev. Mod. Phys. **66**, 1125 (1994).
[6] J. Figueras, T. Puig, X. Obradors, W. K. Kwok, L. Paulius, G. W. Crabtree, and G. Deutscher, Nat. Phys. **2**, 402 (2006).
[7] B. Khaykovich, D. T. Fuchs, K. Teitelbaum, Y. Myasoedov, E. Zeldov, T. Tamegai, S. Ooi, M. Konczykowski, R. A. Doyle, and S. F. W. R. Rycroft, Phys. Rev. B **61**, R9261 (2000).
[8] M. Benkraouda and J. R. Clem, Phys. Rev. B **53**, 438 (1996).
[9] J. W. Guikema, H. Bluhm, D. A. Bonn, R. Liang, W. N. Hardy, and K. A. Moler, Phys. Rev. B **77**, 104515 (2008).
[10] M. Beleggia, G. Pozzi, A. Tonomura, H. Kasai, T. Matsuda, K.

Harada, T. Akashi, T. Masui, and S. Tajima, Phys. Rev. B **70**, 184518 (2004).
[11] A. N. Grigorenko, S. J. Bending, A. E. Koshelev, J. R. Clem, T. Tamegai, and S. Ooi, Phys. Rev. Lett. **89**, 217003 (2002).
[12] V. K. Vlasko-Vlasov, A. Koshelev, U. Welp, G. W. Crabtree, and K. Kadowaki, Phys. Rev. B **66**, 014523 (2002).
[13] A. Moser, H. Hug, B. Stiefel, and H. Guntherodt, J. Magn. Magn. Mater. **190**, 114 (1998).
[14] E. W. J. Straver, J. E. Hoffman, O. M. Auslaender, D. Rugar, and K. A. Moler, Appl. Phys. Lett. **93**, 172514 (2008).
[15] O. M. Auslaender, L. Luan, E. W. J. Straver, J. E. Hoffman, N. C. Koshnick, E. Zeldov, D. A. Bonn, R. Liang, W. N. Hardy, and K. A. Moler, Nat. Phys. **5**, 35 (2009).
[16] T. Schneider, Physica B **326**, 289 (2003).
[17] R. Liang, D. Bonn, and W. Hardy, Physica C **304**, 105 (1998).
[18] A. Hosseini, D. M. Broun, D. E. Sheehy, T. P. Davis, M. Franz, W. N. Hardy, R. Liang, and D. A. Bonn, Phys. Rev. Lett. **93**, 107003 (2004).
[19] D. M. Broun, W. A. Huttema, P. J. Turner, S. Ozcan, B. Morgan, R. Liang, W. N. Hardy, and D. A. Bonn, Phys. Rev. Lett. **99**, 237003 (2007).
[20] R. Liang, D. A. Bonn, W. N. Hardy, and D. Broun, Phys. Rev. Lett. **94**, 117001 (2005).
[21] T. Albrecht, P. Grutter, D. Horne, and D. Rugar, J. Appl. Phys. **69**, 668 (1991).
[22] We used a commercial cantilever Nanosensors™SSS-QMFMR with tip radius of curvature ≈ 25 nm.
[23] J. Sader, J. Chon, and P. Mulvaney, Rev. Sci. Instrum. **70**, 3967 (1999).
[24] J. R. Clem, Physica C **235-240**, 2607 (1994).
[25] The micron-size d_{offset} mostly comes from the sample nonsuperconducting layer, which developed as a result of extensive surface cleaning due to contamination.
[26] D. R. Nelson and V. M. Vinokur, Phys. Rev. B **48**, 13060 (1993).
[27] D. R. Nelson, Phys. Rev. Lett. **60**, 1973 (1988).
[28] C. J. Olson Reichhardt and M. B. Hastings, Phys. Rev. Lett. **92**, 157002 (2004).